Title

The Steady-State Convection-Diffusion Equation at High Peclet Numbers for a Cluster of Spheres: An Extension of Levich's Theory

Journal

SIAM Journal on Applied Mathematics, 76(4)

ISSN

0036-1399 1095-712X

Authors

Biello, Joseph A
Samson, Rene
Sigal, Eugene

Publication Date

2016-08-09

DOI

10.1137/15M1039389

Peer reviewed

SIAM J. APPL. MATH.
Vol. 76, No. 4, pp. 1515–1534

THE STEADY-STATE CONVECTION-DIFFUSION EQUATION AT HIGH PÉCLET NUMBERS FOR A CLUSTER OF SPHERES: AN EXTENSION OF LEVICH'S THEORY*

JOSEPH A. BIELLO†, RENÉ SAMSON‡, AND EUGENE SIGAL§

Abstract. This paper describes an approximate analytical model of competitive effects between members of a dense cluster of absorbing objects, which are modeled as spheres. Neighboring absorbing spheres compete for diffusing species and thereby reduce each other's rate of absorption. Levich's well-known asymptotic (high Péclet number) theory of convection-diffusion considers only the inner region of the concentration boundary layer; it does not describe the wake zone accurately. An extension of the Levich model is constructed for the wake zone. This is used to model intersphere competitive effects. The model demonstrates that for two neighboring spheres aligned along the flow direction, the absorption of the downstream sphere is substantially reduced vis-à-vis the upstream sphere. The model is verified by comparison to numerical simulation studies. Both single-sphere simulations (reported in this paper) and multisphere simulations (taken from existing literature) are considered. In the single-sphere case, the discrepancy between the analytical model and the numerical results is maximally 10% at Pe = 10 and much lower at higher Péclet numbers. An appreciable part of the error stems from the original Levich model itself, rather than from our method of extending the Levich model. In the multisphere case, the difference between the analytical model and the numerical studies is generally less than 30%. At small intersphere separations (say, center-to-center distances < 5 sphere radii), the model tends to overestimate the interference effects. This is related to the fact that flow stagnancy in the space between two closely packed spheres is not taken into account in the model.

Key words. diffusion convection mass-transfer

AMS subject classifications. 76R50, 76M45

DOI. 10.1137/15M1039389

1. Introduction.

Consider a steady-state model of mass transport in which a microscopic species moves toward a collection of macroscopic immobile absorption centers. The motion of the microscopic species consists of a combination of stochastic movements (diffusion) and externally imposed motion by a carrier fluid (convection). The macroscopic absorption centers are assumed to be spheres of which the locations are known and fixed; they are assumed to be all of equal size.

In a recent paper [6] we developed an approximate analytical theory for such a system in the case of pure diffusion and in the case of diffusion combined with a relatively weak convective component. It was found that the range of applicability of the former theory in the convection-diffusion (CD) case was very limited; beyond Péclet numbers of about 0.6, our theory was found to be unreliable. (The Péclet number measures the ratio between convective and diffusive fluxes.) As will be shown below (and as is intuitively quite plausible), the reason for this failure at high Péclet numbers is that CD-concentration profiles around a sphere exhibit an extreme degree of fore/aft asymmetry. At the front side of the sphere, the solute is swept up extremely close to the boundary of the sphere and the concentration gradients are extremely

*Received by the editors September 11, 2015; accepted for publication (in revised form) May 6, 2016; published electronically August 9, 2016.
http://www.siam.org/journals/siap/76-4/M103938.html
†Department of Mathematics, University of California, Davis, CA 95616 (biello@math.ucdavis.edu). The work of this author was supported by U.S. NSF grant NSF-DMS 1313477.
‡Jacob van Lennepkade 29-hs, Amsterdam, 1054 ZE, The Netherlands (rsamsonjvlk@gmail.com).
§Nabla Works, Europaweg 151, Zoetermeer, 2711 ER, The Netherlands (info@nablaworks.com).

steep. At the back side there is an elongated wake zone, where the concentration slowly regains its asymptotic value. This zone can easily extend to distances of well over one hundred times the sphere radius. The use of multipolar expansions was an essential element in our previous paper for finding approximate solutions. For the steady-state diffusion equation, this is a commonly used technique, and in that case our model leads to very accurate approximations (errors much lower than 1%) at the dipolar level. For the CD-equation at high Péclet numbers, it would be unreasonable to expect that this approach would work as well, since the spherical harmonic functions are not a good basis set to represent fields with such extreme fore/aft asymmetry.

In order to construct a multisphere CD theory, it is imperative to fully understand the single-sphere case, in particular with regard to the characteristics of the wake zone. A downstream sphere that is located in the wake of an upstream sphere will "see" a concentration field that is strongly depleted by the upstream sphere. For other two-body configurations (e.g., two spheres that are laterally displaced relative to the flow direction), the mutual influence between absorbers is likely to be much smaller (at high Péclet numbers) than in the case of configurations along the flow direction.

Our paper is organized as follows. In section 2, the single-sphere problem is addressed. Although there is a large amount of work on this subject (see, e.g., [2] for a prominent paper on the low Péclet number problem, and [7] and [11] for reviews of the subject), the current paper focuses on the seminal work of Levich [10] pertaining to the high Péclet number limit. Levich's work deals with the thin mass-transfer boundary layer surrounding an absorbing sphere but cannot be used to describe the wake zone behind the sphere. In section 2, this limitation in Levich's theory is first discussed and subsequently removed, thereby creating an extension to Levich's model that fits seamlessly with the original boundary layer solution. In section 3, the multisphere problem is tackled, building on the ideas developed in section 2. Pairwise interactions between absorbers are described on the basis of the wake field of an upstream absorber. In section 4, results computed by use of the current model are compared against numerical simulation results. In section 4.1, the model is compared against single-sphere numerical data, obtained by use of a commercial, finite-element, general PDE solver (Comsol). In section 4.2, the model is compared against previously published numerical simulation studies of heat or mass transfer to a multiplicity of spheres in a convective flow field [3, 8, 14, 16, 17].

2. Single-sphere problem.

2.1. The Levich solution for the inner field. Consider a single sphere surrounded by a flowing medium spiked with a microscopic solute species with concentration $c(\overrightarrow{r})$. The solute is absorbed by the sphere upon contact with its outer boundary. The steady-state concentration of the solute is given by the convection-diffusion (CD) equation

$$\left(D\ \nabla^2 - \overrightarrow{u}(\overrightarrow{r})\ .\overrightarrow{\nabla}\right)\ c(\overrightarrow{r}) = 0 \tag{2.1}$$

with the boundary conditions

$$c(\overrightarrow{r}) \to c_0 \quad \text{as} \quad r \to \infty \tag{2.2}$$

and

$$c(\overrightarrow{r}) = 0 \quad \text{when} \quad r = a. \tag{2.3}$$

Here, a is the sphere radius and D is the diffusion constant of the solute in the flow medium. The velocity field $\overrightarrow{u}(\overrightarrow{r})$ is assumed to be *known*; $c(\overrightarrow{r})$ is the concentration field that is to be computed.

In [6] it was assumed that the velocity field is constant and unidirectional everywhere in space outside the sphere (for another series of papers that is also based on a constant velocity field, we refer the reader to [9, 12, 13]). This choice, however, leads to unrealistic mass distributions. Hence, a different choice is now made for the flow field. Instead we shall consider laminar flow.

In his 1962 book *Physicochemical Hydrodynamics* [10], Levich presented an ingenious solution method for the CD-equation in the case of low-Reynolds-number/high-Péclet-number flow around a sphere, which we summarize below. First, the CD-equation is cast in dimensionless form. Taking the sphere radius a as the unit of length, the asymptotic concentration c_0 as the unit of concentration and the asymptotic (scalar) velocity u_0 as the unit of velocity, (2.1)–(2.3) become

$$\left(\nabla^2 - \frac{1}{\epsilon}\overrightarrow{u}(\overrightarrow{r})\,.\overrightarrow{\nabla}\right)\; c(\overrightarrow{r}) = 0 \tag{2.4}$$

with

$$c(\overrightarrow{r}) \to 1 \quad \text{as} \quad r \to \infty \tag{2.5}$$

$$c(\overrightarrow{r}) = 0 \quad \text{when} \quad r = 1, \tag{2.6}$$

and

$$\frac{1}{\epsilon} = \mathrm{Pe} = \frac{u_0\; a}{D}. \tag{2.7}$$

Pe is the Péclet number. The reader is cautioned that with this definition, Pe is 2 times larger than the variable η used in our previous publication [6] and half as large as the Péclet number as used in many engineering texts (which usually take the sphere's diameter rather than its radius as the unit of length).

Following Levich, we are primarily interested in the case that $\mathrm{Pe} \gg 1$, in other words, that $\epsilon \ll 1$. Levich argues that when $\mathrm{Pe} \gg 1$, a narrow concentration boundary layer exists close to the surface of the sphere, where the concentration decreases steeply from its asymptotic value on the outer edge of the layer to naught on the sphere's surface. The rapid decay of c within a radial distance that is much smaller than the radius of the sphere is strictly speaking only true on the upstream and not on the downstream side. Nevertheless, on the basis of this assumption, Levich derives an approximation to the CD-equation which can be solved analytically. His solution has the form

$$c(\overrightarrow{r}) = c_{in}(r,\theta) = \frac{1}{\gamma_0}\int_0^{\zeta(r,\theta)} \exp\left[-\frac{4s^3}{9}\right]\; ds = 1 - \frac{\Gamma(1/3, (4/9)\;\zeta(r,\theta)^3)}{\Gamma(1/3)}, \tag{2.8}$$

where

$$\zeta(r,\theta) = \left[\frac{3}{4\epsilon}\right]^{1/3} \frac{(r-1)\sin(\theta)}{\left[\pi - \theta + \frac{1}{2}\sin(2\theta)\right]^{1/3}} \tag{2.9}$$

and

$$\gamma_0 = \frac{\Gamma\,(1/3)}{12^{1/3}}. \tag{2.10}$$

Here, r and θ are the radial and the polar-angular coordinates of the spherical coordinate system. The sphere is centered on the origin of the coordinate system. The flow is directed along the z-axis, pointing in the positive z-direction. The point $z = -1$ ($\theta = \pi$) on the z-axis is the stagnation point of the flow on the surface of the sphere. In (2.8) the integral is expressed in terms of the incomplete gamma function $\Gamma(\alpha, x)$ and the complete gamma function $\Gamma(\alpha)$; see [1].

Figure 1(a) shows a contour plot of the Levich solution for Pe = 100. A two-dimensional projection is shown in the $\{x, z\}$-plane. The solution is rotation-symmetric around the z-axis, so only the sector $x > 0$ needs to be shown. On the upstream side of the sphere, the boundary layer is extremely narrow, as expected. On the downstream side, the Levich solution exhibits an infinitely long tail around the positive z-axis. In the transverse direction (perpendicular to the z-axis), there is a steep concentration gradient, with an unphysical gradient discontinuity at $\rho = 0$ (ρ being the distance to the z-axis), as was pointed out before by many authors (see, for example, [5] and [7]). Concentration gradients must be "washed away" at a sufficiently large distance from the sphere through the action of diffusion. This is absent in the solution shown in Figure 1(a).

The discontinuity in the concentration gradient at $\rho = 0$ is both counterintuitive and harmful for the further development of a theory encompassing intersphere effects. We shall have to correct this before we can proceed to multisphere interactions.

2.2. Correction to the Levich solution in the wake zone: The outer field. The following development is best formulated in terms of cylindrical (rather than in spherical) coordinates, denoted by the symbols $\{\rho, z, \varphi\}$. Here, ρ is the distance to the z-axis (not to be confused with r, the distance to the origin). The azimuthal angle φ is irrelevant here, because of the axial symmetry of the problem.

The extension of the CD-equation to the wake zone is closely fashioned after Levich's method for the inner field. The development hinges on the notion that in the wake zone, local coordinates along the stream lines and local coordinates orthogonal to stream lines play two quintessentially distinct roles in the physics of the mass-transfer process. The coordinate along the stream lines is primarily associated with advection; i.e., clusters of solute particles are carried along by the flow *as a coherent patch* with hardly any distortion. By contrast, the coordinate orthogonal to the stream lines is most actively involved in the diffusional mixing.

The so-called Stokes stream function for flow past a sphere [4] is (in dimensionless units)

$$\psi = \frac{\rho^2}{2}\left[1 - \frac{3}{2r} + \frac{1}{2r^3}\right], \tag{2.11}$$

where

$$r^2 = \rho^2 + z^2\ ; \qquad \rho = r\ \sin(\theta)\ ; \quad z = r\ \cos(\theta). \tag{2.12}$$

In cylindrical coordinates, the velocity vector $\overrightarrow{u}$ is related to the stream function ψ as follows:

$$\overrightarrow{u} = \frac{1}{\rho}\left[\frac{\partial\psi}{\partial\rho}\hat{z} - \frac{\partial\psi}{\partial z}\hat{\rho}\right]. \tag{2.13}$$

The equation that is to be solved is the CD-equation

$$\frac{1}{\rho}\frac{\partial}{\partial\rho}\left(\rho\frac{\partial c}{\partial\rho}\right) + \frac{\partial^2 c}{\partial z^2} - \frac{1}{\epsilon\rho}\left[\frac{\partial\psi}{\partial\rho}\frac{\partial c}{\partial z} - \frac{\partial\psi}{\partial z}\frac{\partial c}{\partial\rho}\right] = 0 \tag{2.14}$$

in the domain $z \geq 1$. Apart from the asymptotic boundary condition (2.5), a condition is imposed on the plane $z = 1$ to guarantee continuity between the inner and outer fields; more details about this latter boundary condition are specified below.

Following Levich, a coordinate transformation is now made from the system $\{\rho, z\}$ to $\{\psi, Z\}$ with $Z = z$. The transformation rules for the first derivative are as follows:

$$\left.\frac{\partial}{\partial\rho}\right|_z = \left.\frac{\partial\psi}{\partial\rho}\right|_z \left.\frac{\partial}{\partial\psi}\right|_Z + \left.\frac{\partial Z}{\partial\rho}\right|_z \left.\frac{\partial}{\partial Z}\right|_\psi = \left.\frac{\partial\psi}{\partial\rho}\right|_z \left.\frac{\partial}{\partial\psi}\right|_Z, \tag{2.15}$$
$$\left.\frac{\partial}{\partial z}\right|_\rho = \left.\frac{\partial\psi}{\partial z}\right|_\rho \left.\frac{\partial}{\partial\psi}\right|_Z + \left.\frac{\partial Z}{\partial z}\right|_\rho \left.\frac{\partial}{\partial Z}\right|_\psi = \left.\frac{\partial\psi}{\partial z}\right|_\rho \left.\frac{\partial}{\partial\psi}\right|_Z + \left.\frac{\partial}{\partial Z}\right|_\psi.$$

In the transformed variables, the only term surviving in the advective term is

$$\vec{u} \cdot \vec{\nabla} c = \frac{1}{\rho}\frac{\partial\psi}{\partial\rho} \left.\frac{\partial c}{\partial Z}\right|_\psi, \tag{2.16}$$

while the radial diffusion term becomes

$$\frac{1}{\rho}\frac{\partial}{\partial\rho}\left(\rho\frac{\partial c}{\partial\rho}\right) = \frac{1}{\rho}\left(\frac{\partial\psi}{\partial\rho}\right) \frac{\partial}{\partial\psi}\left[\rho\left(\frac{\partial\psi}{\partial\rho}\right) \left.\frac{\partial c}{\partial\psi}\right|_Z\right]\Bigg|_Z. \tag{2.17}$$

Substituting (2.16) and (2.17) into (2.14), we obtain

$$\frac{1}{\rho}\frac{\partial\psi}{\partial\rho}\left\{\frac{\partial}{\partial\psi}\left[\rho\left(\frac{\partial\psi}{\partial\rho}\right) \left.\frac{\partial c}{\partial\psi}\right|_Z\right]\Bigg|_Z - \frac{1}{\epsilon}\left.\frac{\partial c}{\partial Z}\right|_\psi\right\} + \frac{\partial^2 c}{\partial z^2} = 0, \tag{2.18}$$

where the axial diffusion term, $\partial^2 c/\partial z^2$, is not explicitly transformed in terms of the variables ψ and Z.

Consider the limit $\epsilon \to 0$. In Appendix A it is shown that in this limit the term $\partial^2 c/\partial z^2$ is negligible. Under this assumption, it is clear that everywhere in the domain where $u_z = (1/\rho)(\partial\psi/\partial\rho) \neq 0$, the factor in curly brackets must be zero. Note that u_z (the axial component of the velocity vector) $= 0$ on the boundary of the sphere and $\neq 0$ everywhere else. Hence, the dominant balance in the limit $\epsilon \to 0$ is the approximate equation

$$\frac{\partial}{\partial\psi}\left[\rho\frac{\partial\psi}{\partial\rho}\frac{\partial c}{\partial\psi}\right] - \frac{1}{\epsilon}\frac{\partial c}{\partial z} = 0. \tag{2.19}$$

Henceforth, the distinction between z and Z is ignored, lowercase z is used throughout, and the designation which variable is to be kept constant during differentiation is dropped, with the cautionary remark that the differential $\partial/\partial z$ is to be taken at constant ψ.

The factor $\rho\,\partial\psi/\partial\rho$ can be written as

$$\rho\frac{\partial\psi}{\partial\rho} = 2\psi + P(\rho, z), \tag{2.20}$$

where

$$P(\rho, z) = \frac{3}{4}\frac{\rho^4(\rho^2 + z^2 - 1)}{(\rho^2 + z^2)^{5/2}}. \tag{2.21}$$

We now consider the ratio $P(\rho,z)/2\psi$ in the region $\{z \geq 2, \rho \leq 1\}$. This is the region of major interest in the study of interacting absorbers. In that region, the maximal value of $P(\rho,z)/2\psi$ is 0.143..., attained on the bounding circle $\{z = 2, \rho = 1\}$. More particularly, we shall be interested in the region quite close to or at the z-axis. As $\rho \to 0$, $P(\rho,z)/2\psi \to 0$, as ρ^2. In conclusion, for the region of practical interest, it is an excellent approximation to assume that $\rho\frac{\partial\psi}{\partial\rho} \approx 2\psi$ so that (2.19) can be simplified to

$$\frac{\partial}{\partial\psi}\left[2\psi\frac{\partial c}{\partial\psi}\right] = \frac{1}{\epsilon}\frac{\partial c}{\partial z}. \tag{2.22}$$

Consider the following coordinate transformation:

$$u = \sqrt{2\psi}\cos(\lambda)\ ; \quad v = \sqrt{2\psi}\sin(\lambda)\ . \tag{2.23}$$

If the concentration is assumed to be independent of the angular coordinate λ, then it is simple to show that (2.22) becomes

$$\frac{1}{\epsilon}\frac{\partial c}{\partial z} = \frac{\partial^2 c}{\partial u^2} + \frac{\partial^2 c}{\partial v^2}, \tag{2.24}$$

which is a two-dimensional nonstationary diffusion equation in two space-like coordinates $\{u, v\}$ and a time-like coordinate z.

Consider the Green's function of (2.24) in $z > z_0$:

$$G(u,v,z) = \frac{\exp\left[-\frac{u^2+v^2}{4\epsilon z}\right]}{4\pi\,\epsilon\,z}. \tag{2.25}$$

Equation (2.24) can now be solved as a convolution of initial data at $z = z_0$ with the Green's function. If initial data at $z = z_0$ are known,

$$c(u,v,z_0) = C_0(u,v), \tag{2.26}$$

then the solution of (2.24) for $z > z_0$ is

$$\begin{aligned} c(u,v,z) &= \int_{-\infty}^{\infty}\int_{-\infty}^{\infty} C_0(u',v')G(u-u',v-v',z-z_0)\,du'\,dv' \\ &= \int_{-\infty}^{\infty}\int_{-\infty}^{\infty} C_0(u',v')\,\frac{\exp\left[-\frac{(u-u')^2+(v-v')^2}{4\epsilon(z-z_0)}\right]}{4\pi\,\epsilon\,(z-z_0)}\,du'\,dv'. \end{aligned} \tag{2.27}$$

The double integral can be simplified by transforming back from $\{u, v\}$ to $\{\psi, \lambda\}$. Note that the Jacobian of the transformation is unity, so that the transformed integral becomes

$$c(u,v,z) = \frac{e^{\left[-\frac{\psi}{2\epsilon(z-z_0)}\right]}}{4\pi\,\epsilon\,(z-z_0)}\int_0^{2\pi}\int_0^{\infty} C_0(u',v')\,e^{\left[\frac{u\,u'+v\,v'}{2\epsilon(z-z_0)}\right]}e^{\left[-\frac{\psi'}{2\epsilon(z-z_0)}\right]}\ d\psi'\,d\lambda'. \tag{2.28}$$

The cross term in the exponential is simplified by using

$$u\,u' + v\,v' = 2\sqrt{\psi\,\psi'}\cos(\lambda-\lambda'). \tag{2.29}$$

As initial data $C_0(u,v)$, we shall use the cross-section of the Levich inner solution—(2.8)—with the plane $z = 1$. (The justification for this choice is discussed in section

4.1 below.) This cross-section is circularly symmetric around the point $\{z = 1, \rho = 0\}$ (the north pole of the sphere). Using this circular symmetry, we may write

$$C_0(u', v') = c_0(\psi'). \tag{2.30}$$

Hence, the angular integral only concerns the exponential cross term, and the following equality can be used (see [1]):

$$\frac{1}{2\pi}\int_0^{2\pi} \exp\left[s\cos(\lambda')\right]\, d\lambda' = I_0\left(s\right), \tag{2.31}$$

where $I_0\left(s\right)$ is the modified spherical Bessel function of order zero (see [1]). Therefore, the expression for the concentration is independent of the angle λ (as it must be!) and becomes

$$c_{out}(\psi, z) = \frac{\exp\left[-\frac{\psi}{2\epsilon(z-z_0)}\right]}{2\epsilon\left(z - z_0\right)} \int_0^{\infty} c_0(\psi')\; I_0\left(\frac{\sqrt{\psi\,\psi'}}{\epsilon(z-z_0)}\right) \exp\left[-\frac{\psi'}{2\epsilon(z-z_0)}\right]\quad d\psi'. \tag{2.32}$$

We still need to specify how to compute $c_0(\psi)$. In (2.8)–(2.10), Levich's concentration field is expressed in terms of spherical polar coordinates. It must now be expressed in terms of the variables ψ and z. This is achieved as follows. First, c_0 is expressed in the cylindrical coordinate ρ at $z = z_0$:

$$c_0(\rho, z_0) = \frac{1}{\gamma_0}\int_0^{\zeta(\rho,z_0)} \; e^{-\frac{4}{9}z^3}\; dz\;; \quad \gamma_0 = \frac{\Gamma\left(1/3\right)}{12^{1/3}}, \tag{2.33}$$

where

$$\zeta(\rho, z_0) = \zeta(\rho, 1) = \left[\frac{3}{4\,\epsilon}\right]^{\frac{1}{3}} \frac{\rho - \frac{\rho}{\sqrt{\rho^2+1}}}{\left[\pi - \arccos\left\{\frac{1}{\sqrt{\rho^2+1}}\right\} + \frac{\rho}{\sqrt{\rho^2+1}}\right]^{\frac{1}{3}}}. \tag{2.34}$$

Second, given a value of ψ' (the integration variable in (2.32)), the corresponding value of ρ to be used in the calculation of $c_0(\psi')$ is given by

$$\rho = \sqrt{\frac{2\psi'}{1 - \frac{3}{2r_0} + \frac{1}{2r_0^3}}}\quad ; \quad r_0 = \sqrt{\rho^2 + z_0^2} = \sqrt{\rho^2 + 1}. \tag{2.35}$$

This is an implicit equation for ρ that is easily solved numerically.

Figures 1(b) and 1(c) show contour plots for Pe = 10 and 100. The function plotted is equal to c_{out} (equation (2.32)) for $z > 1$ and c_{in} (equation (2.8)) for $z \leq 1$. Note that there is a seamless match between the inner and outer solutions at $z = 1$. The horizontal and vertical axes in the plots are ρ and z, respectively, expressed in units of sphere radius. Comparing these plots with the inner solution (see Figure 1(a)), it is clear that the problematic aspects of the inner solution in the wake zone have now disappeared: the gradient discontinuity at the positive z-axis is absent and the benevolent action of diffusion is clearly present: along the z-axis and elsewhere, the concentration gradually approaches its asymptotic value (equal to 1) as one moves farther away from the sphere. As expected, this happens faster at Pe = 10 (Figure 1(b)) than at Pe = 100 (Figure 1(c)).

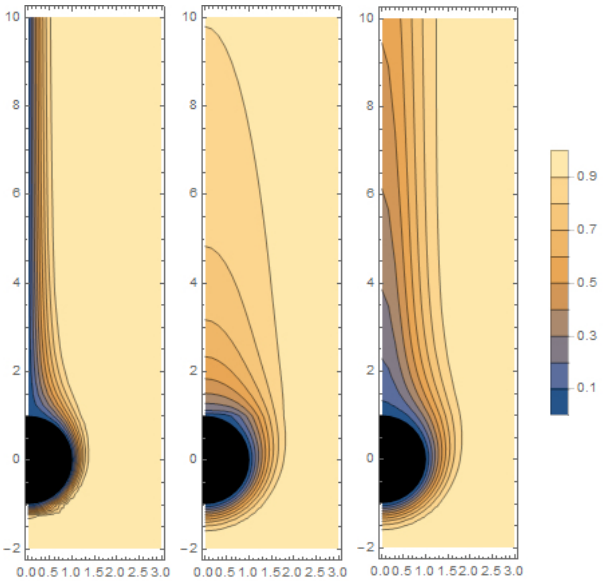

FIG. 1. *Contour plots for concentration fields.* (a) *Original Levich solution* (2.8) *for* Pe = 100*;* (b),(c) *Extended Levich solution* (2.32) *for* Pe = 10 *and* 100.

3. Multisphere problem. The question to be addressed now is how to use the single-sphere's concentration field to model competitive effects between two (or more) spheres. A brief review is given below of the methodology developed in our previous paper [6]. A crucial ingredient in this method is the knowledge of a Green's function for the corresponding equation. It is shown below how the same concept can be used in the current case, using the single-sphere (outer) concentration field instead of the Green's function.

In [6] it was shown how the monopolar approximation can be used to get a lowest order theory for a collection of absorbing spheres in the limit of a small Péclet number. The monopolar theory amounts to solving the following linear system of equations (one equation for each sphere in the ensemble):

$$1 = \sum_{j=1}^{N} \Phi_{ij}\ q_j \qquad \forall i = 1, \ldots, N, \tag{3.1}$$

where the "charge" q_j is related to the mass flux of solute into the sphere labeled j, and $\Phi_{ij} = \Phi(\overrightarrow{r_i} - \overrightarrow{r_j})$ is the Green's function for a charge located at $\overrightarrow{r_j}$ acting on a charge located at $\overrightarrow{r_i}$.

Even though we do not have a Green's function for the CD-equation with Stokes flow, it is very tempting to employ the wake function (2.32) for just that purpose. Apart from a trivial modification, the computed "wake" field has exactly the same physical content as the Green's function. It describes the effect of a single absorber on the concentration field in its surroundings. The only modification we need to make is to work with the function $(1 - c)$ rather than with c itself, so that we have the required asymptotic behavior at ∞ (asymptotic decay to zero rather than to one).

By analogy to (3.1) we now consider the linear system of equations

$$1 = \sum_{j=1}^{N} \Omega_{ij}\ q_j \qquad \forall i = 1, \ldots, N, \tag{3.2}$$

where

$$\Omega_{ij} = \delta_{ij} + (1 - \delta_{ij}) * \begin{cases} 1 - c_{out}(\vec{r}_i - \vec{r}_j) & \text{if} \quad z_j < z_i, \\ 0 & \text{if} \quad z_j > z_i, \end{cases} \tag{3.3}$$

where δ_{ij} is the Kronecker-delta matrix, $\overrightarrow{r_j}$ is the coordinate of the center of sphere j, and z_j is its z-coordinate.

Consider an assembly of two spheres placed along the z-axis in order of increasing z-coordinates ($z_1 < z_2$). The matrix Ω then has a lower-triangular form,

$$\Omega = \begin{pmatrix} 1 & 0 \\ \omega_{21} & 1 \end{pmatrix}, \tag{3.4}$$

where

$$\omega_{21} = 1 - c_{out}(\overrightarrow{r_2} - \overrightarrow{r_1}). \tag{3.5}$$

Our goal is to compute the "charges" q_1 and q_2 which are really the (nondimensional) flux rates to spheres 1 and 2. From (3.2) it follows that

$$\overline{q} = \begin{pmatrix} q_1 \\ q_2 \end{pmatrix} = \overline{\overline{\Omega^{-1}}}\ \ \overline{1} = \begin{pmatrix} 1 & 0 \\ -\omega_{21} & 1 \end{pmatrix} \begin{pmatrix} 1 \\ 1 \end{pmatrix} = \begin{pmatrix} 1 \\ c_{out}(\overrightarrow{r_2} - \overrightarrow{r_1}) \end{pmatrix}. \tag{3.6}$$

As expected, sphere #1, which is in the upstream location, is not affected by sphere #2 (hence, $q_1 = 1$), while sphere #2, which is located in the wake of sphere #1, has a reduced absorption ($q_2 < 1$) given by $c_{out}(\overrightarrow{r_2} - \overrightarrow{r_1})$, because its feed stream has been partly eaten up by sphere #1. The farther the two spheres are apart, the more the feed stream to sphere #2 is replenished by diffusion and the more q_2 approaches 1.

Figure 2 shows computed results. Here, the two spheres are colinear with the z-axis; their mutual distance is given by z (the horizontal plot axis); the Péclet number varies from 10 to 1000. The vertical plot axis is q_2, the normalized absorption rate of the second (downstream) sphere. Figure 2(a) plots the z-range from 2 to 100; Figure 2(b) zooms in on the z-range from 2 to 10. The curves are in order of increasing Péclet number, as one would expect. The higher the Péclet number, the stronger the depletion of solute in the wake zone close to the rear side of sphere #1 (the upstream sphere) and the longer it takes before this deficit is ironed out by the equalizing effect of diffusion. For high Péclet number, a substantial distance from the upstream sphere is required before almost-complete replenishment of solute (c close to 1) is achieved.

In Figure 3 an assembly of three spheres is considered, where sphere #1 is centered at the origin, sphere #3 at $\{\rho = 0, z = 6\}$, and sphere #2 at $\{\rho = variable,\ z = 3\}$; in other words, the centers of the spheres form an isosceles triangle in which spheres #1 and #3 are aligned along the z-axis and #2 is halfway between #1 and #3 but shifted away from the z-axis by a variable amount. The plot shows how q_2 and q_3 change as a function of the ρ-coordinate of sphere #2. The Péclet number = 10. When sphere #2 is shifted by about 2.5 times the sphere radius, it is completely outside

the zone of influence of sphere #1, and its q-value is almost equal to 1, as expected. As long as the ρ-shift of sphere #2 is < 2.5, sphere #3 feels the competitive effect of *both* upstream spheres (both #1 and #2). When sphere #2 is sufficiently far away from the z-axis, sphere #3 doesn't feel its influence anymore, but the effect of #1 is undiminished of course. This is why q_3 tends to an asymptote that is < 1.

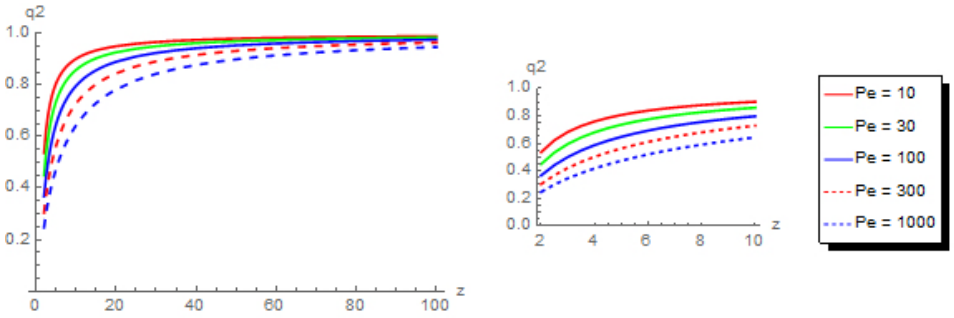

(a) (b)

FIG. 2. (a) *Dimensionless rate of absorption by a sphere that is shielded from the flow by another sphere at an upstream location. Horizontal plot axis* z = *intersphere distance in units of sphere radii.* (b) *Same plot for* z *ranging from* 2 *to* 10.

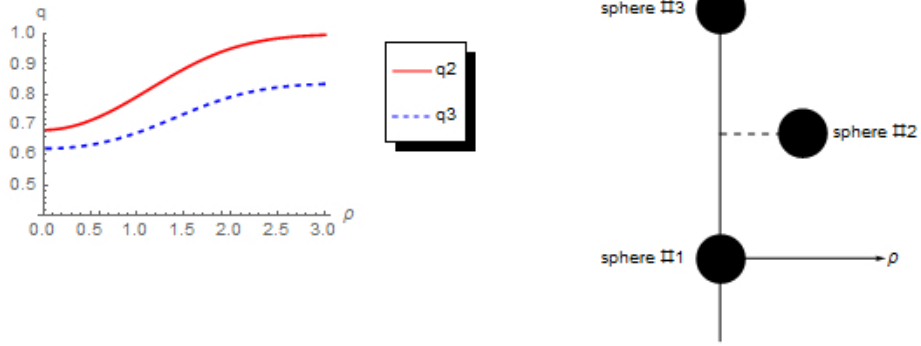

FIG. 3. *Plot of the rates of absorption* q_2 *and* q_3 *in a cluster of three spheres arranged in an isosceles triangle. Sphere #2 is displaced from the z-axis by an amount given by the* ρ*-coordinate (= the horizontal plot axis).* Pe = 10.

4. Model validation.

4.1. Numerical validation of the single-sphere model. In order to validate the single-sphere model presented in section 2, numerical simulation studies were carried out in which the CD-equation (without any approximations) around a single sphere in a Stokesian flow field was solved with the same boundary conditions as before. Numerical solutions were obtained using a general-purpose commercial finite-

element software package—Comsol Multiphysics—which is frequently used in scientific and engineering applications.

In order to satisfy the boundary condition at infinity, so-called infinite elements were used for the outer computational domain. Infinite domains are often a challenge in finite-element simulations. One way of tackling this problem is to surround a "large enough" bounded domain by an infinite region with suitably chosen scaled coordinates. The size of the inner region was chosen through a convergence study to ensure sufficient solution accuracy. Since the solution on the boundary of the "inner" domain is already quite close to the asymptotic value, the gradient in the outer region can be modeled as a simple parametrized function of the scaled coordinate. For more details on this subject, see [18].

Two aspects of the numerical model were varied to ensure convergence: the size of the computational domain (excluding the infinite elements) and the size and the number of mesh elements. The mesh elements were densely distributed in regions where concentration gradients were large and were more sparsely distributed in regions of low concentration gradients. In order to achieve high, uniform accuracy, the distribution of the mesh elements was prescribed using a priori knowledge of the structure of the solution.

It was found that a spherical domain of radius 200 (expressed in the basic unit length of one absorber sphere radius) containing about 800,000 second-order mesh elements was sufficient to satisfy accuracy requirements. The accuracy requirements were formulated as follows. A number of marker points were distributed in the computational domain. For convergence, it was stipulated that the calculated values at each of these marker points should vary by less than 10^{-3} between computations with successively higher resolutions. Computations were carried out for Pe values of 10, 100, and 1000, and there were no convergence difficulties in any of these runs.

We introduce the following four metrics to compare the analytical and numerical solutions:

$$\varepsilon_i = \max(c_A - c_N)|_{\Omega_i} \qquad (i = 1, 2), \tag{4.1}$$

$$\varepsilon_3 = \left[\frac{\int_{\Omega_1} dz\ d\rho\ (c_A - c_N)^2}{\int_{\Omega_1} dz\ d\rho\ \left[1 - 0.5 * (c_A + c_N)\right]^2} \right]^{1/2}, \tag{4.2}$$

and

$$\varepsilon_4 = \frac{|c_A - c_N|}{c_N}. \tag{4.3}$$

c_A and c_N are the analytical and the numerical solutions, respectively. Ω_1 and Ω_2 are two domains on which the solutions are computed. Ω_1 is the cylindrical domain between $z = [-2, +37.5]$ and $\rho < 3$, excluding the central sphere ($r < 1$). The domain Ω_2 is defined as $\{+2 < z < 37.5\ \&\ \rho < 3\}$ and focuses on the wake zone. ε_1 and ε_2 measure the maximum difference between c_A and c_N on Ω_1 and Ω_2, respectively. ε_3 represents an integral comparison norm on Ω_1. The function $(1 - c)$ is integrable over the infinite domain, and we compare the numerical and analytical values of this function in the normalized L^2 sense.

Figure 4(a) shows a contour plot of the concentration difference $(c_A - c_N)$ on Ω_1 for Pe = 10. It shows that the region of large difference between the two data sets is close to the surface of the central sphere, and the maximal difference is approximately

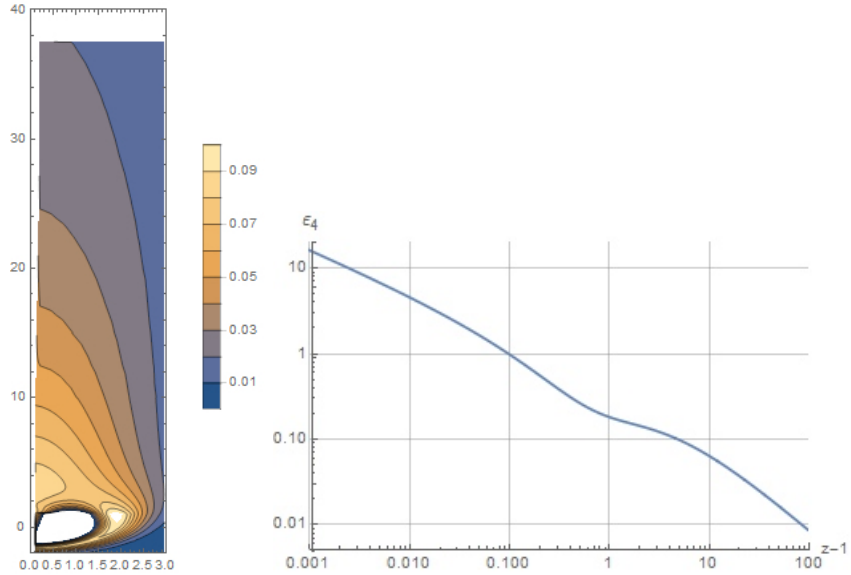

FIG. 4. (a) *Contour plot of the absolute difference between the analytical and the numerical solution for* Pe = 10. (b) *Relative difference between the analytical and the numerical solution for* Pe = 10 *along the positive z-axis. (The horizontal plot axis represents* $z - 1$*.)*

+10% (the analytical data are systematically *higher* than the numerical data). At larger distances from the sphere, the difference decreases to a few percent. Contour plots for the higher Péclet numbers have the same general appearance as for Pe = 10, except that they "hug" the z-axis more closely and are generally lower in the whole domain.

Figure 4(b) shows the *relative* difference between the analytical and the numerical solutions as defined by the comparison norm ϵ_4. This is a log-log line plot along the z-axis. It is clear that close to the surface of the sphere, where *both* solutions rapidly tend to zero, the differences are quite substantial. However, for $z > 2$, $\epsilon_4 < 0.2$ and rapidly tends to smaller values as z increases.

Table 1 lists the comparison norms ε_1 and ε_2 for Péclet values of 10, 100, and 1000. The results are quite satisfactory for Pe = 10 and become even better at Pe = 100 and 1000. The reduction of all the comparison norms with increasing Pe is just what we expect from an asymptotic theory, valid at high Péclet numbers. Qualitatively, the same behavior is observed for the original Levich model; see, e.g., Figure 3.10 of [7].

One detail of our analytical model that was not discussed in section 2 was the rationale for choosing the location of the plane at which the "inner" and the "outer" solution are stitched together. The outputs of analytical runs with different choices for the position of the patching plane were compared with numerical data. The following conclusions were drawn:

(a) For positions of the patching plane in the range $z_0 = [-1, +1]$, the difference between the analytical model and the numerical model became smaller as $z_0 \to 1$.

(b) For positions of the patching plane $z_0 > 1$, although there was a minor improvement of the concentration field at $z > z_0$, there also was a deterioration

TABLE 1
Comparison norms for the single-sphere model as a function of Pe.

Pe	ε_1	ε_2	ε_3
10	0.11	0.086	0.25
100	0.067	0.063	0.14
1000	0.044	0.042	0.089

of the concentration field in the region below the patching plane. This included the occurrence of the embarrassing gradient discontinuity at the z-axis that is inherent in the original Levich solution, which was one of the reasons for constructing the current theory in the first place.

By choosing the position of the patching plane at $z_0 = 1$, we are recognizing the above facts and patching the inner and the outer solution as close as possible to the Levich boundary layer around the sphere.

A feature of Figure 4(a) that merits further comment is the following. From the figure it can be seen that the zone where the difference between the model and the numerics is maximal is very near the $z = 1$ plane. This leads us to the conclusion that an appreciable part of the error in our model stems from the original Levich model itself, rather than from our method of extending the Levich model.

A qualitative difference between an analytical result such as our (2.32) and numerical simulations that should be pointed out is the following: whereas our (2.32) permits calculation of the concentration at a *single field point*, such a calculation is impossible in a numerical scheme, where a *complete mesh* must be created, and concentration values must be calculated at each mesh node. This advantage may seem insignificant for axisymmetric problems, but it becomes critical for three-dimensional problems because accurate three-dimensional solutions may require significant computational resources.

Furthermore, the analytical model is very well suited for open domains because the boundary conditions at infinity are inherently satisfied. A finite-element method, on the other hand, is better suited for closed domains and provides only approximate solutions on open domains. Open-domain finite-element modeling techniques require convergence studies in order to ensure solution accuracy as a function of the model's spatial extent (i.e., convergence as a function of model size).

4.2. Numerical validation of the multisphere model. Below, we compare the output of the model with a number of numerical simulation studies [3, 8, 14, 16, 17]. Interpretation and discussion of the results is postponed to section 4.2.1 below. The reader is advised to refer to Appendix B for details about the nomenclature.

Tal, Lee, and Sirignano (TLS) [16] have studied the linearized Navier–Stokes equation and the enthalpy equation for a pair of spheres aligned along the asymptotic flow direction. For the equation of creeping motion they used an *exact* analytical solution in terms of bispherical coordinates (the Stimson–Jeffery solution) [15]. For the enthalpy equation, a numerical solution (finite differences) was computed. In their calculations, the Reynolds number was 40 (Re based on sphere diameter), the Prandtl number was 1, and the distance between the spheres varied. Table 2 compares their calculated heat transfer results with the extended Levich (EL) model. The difference between their basic length unit and ours (sphere diameter vs. sphere radius) has to be taken into account. Table 2 (and all following tables) uses the definitions and terminology of the current paper (i.e., the length unit and Péclet numbers are based on sphere *radius*).

TABLE 2

Nondimensional rate of absorption for a pair of spheres along the flow direction. Pe = 20 *(basis sphere radius).* z = *the intersphere distance (basis sphere radius). The TLS data refer to* [16]*, the EL data to the current model.*

	$z = 2.4$		$z = 5$	
	q_{TLS}	q_{EL}	q_{TLS}	q_{EL}
Upstream sphere	0.85	1	0.95	1
Downstream sphere	0.53	0.55	0.63	0.76

TABLE 3

Nondimensional rate of absorption for a triplet of spheres along the flow direction. Pe = *variable (basis sphere radius).* $z_{12} = 4$; $z_{23} = 4$ *(in units of sphere radii). The RKW data refer to* [14]*, the EL data to the current model.*

Pe	q_2^{RKW}	q_2^{EL}	q_3^{RKW}	q_3^{EL}
5	0.79	0.80	0.63	0.75
25	0.69	0.69	0.57	0.62
50	0.65	0.64	0.55	0.57
250	0.57	0.51	0.50	0.44
500	0.54	0.46	0.48	0.40
1000	0.51	0.42	0.46	0.35

Ramachandran, Kleinstreuer, and Wang (RKW) [14] have carried out numerical studies of the Navier–Stokes and the enthalpy equation for a *triplet* of spheres centered along a straight line parallel to the flow direction. The range of variables they studied was $1 \leq \mathrm{Re} \leq 200$, $0.1 \leq \mathrm{Pr} \leq 10$, and intersphere distances between 2 and 10 (based on units of sphere diameters). The authors cast their results in the form of correlations that describe the dependence of the calculated Nusselt numbers on Re, Pr, and the intersphere spacings. In order to stay within the range of validity of these correlations, we focused on the combination Pr = 10 with the following list of Reynolds numbers: $\mathrm{Re} = \{0.5, 2.5, 5, 25, 50, 100\}$ (based on sphere radius).

Data comparing the two models are listed in Table 3. The intersphere distances z_{12} and z_{23} are both taken equal to 4 sphere radii. The tabulated values q_2 and q_3 are the integrated flux rates (Nusselt numbers) of spheres #2 and #3, normalized by the q-value of the leading sphere (q_1). These values are listed for the RKW data and for the EL model, respectively.

Aminzadeh et al. (AACKP) [3] solved the conservation-of-species equation numerically for a pair of spheres aligned along the flow direction using the Stimson–Jeffery [15] velocity field. Their simulations covered Péclet numbers up to 50 (based on sphere diameter). In Table 4 our model results (EL) are compared with their computed data for various values of the intersphere separation and the Péclet number. Tabulated is the ratio between the integrated mass-flux of the downstream and the upstream spheres (q_2/q_1). The tabulated AACKP data had to be visually read off the published plots, so the listed data entries may not be very accurate.

Tsai and Sterling [17] have done numerical simulations of the combustion of linear droplet arrays arranged along the flow direction. Their studies covered a Péclet range (based on sphere diameter) from 10 to 120. Assuming a Prandtl number of around 1, the Re range was around 10–120. Their main focus was on heat transfer calculations (Nusselt numbers). Table 5 shows comparative data for two droplets aligned along the flow direction at a spacing of 4 sphere radii and at variable Pe number. The absorption data are the ratio between the flux of the trailing sphere to that of the leading sphere.

TABLE 4

Nondimensional rate of absorption for a pair of spheres along the flow direction. Pe = *variable (basis sphere radius).* z = *the intersphere distance (in units of sphere radii). The AACKP data refer to* [3]*, the EL data to the current model.*

Pe	$z = 2.0$		$z = 3.1$		$z = 8.3$	
	q_{AACKP}	q_{EL}	q_{AACKP}	q_{EL}	q_{AACKP}	q_{EL}
1.25	0.85	0.71	0.80	0.83	0.90	0.94
2.5	0.76	0.66	0.78	0.79	0.89	0.93
5	0.73	0.60	0.76	0.74	0.87	0.91
25	0.71	0.47	0.70	0.62	0.84	0.84

TABLE 5

Nondimensional rate of absorption for two spheres along the flow direction. Pe = *variable (basis sphere radius).* $z_{12} = 4$ *(in units of sphere radii). The TS data refer to* [17]*, the EL data to the current model.*

Pe	q_{TS}	q_{EL}
5	0.73	0.80
15	0.62	0.73
30	0.61	0.68
45	0.58	0.65
60	0.58	0.63

TABLE 6

Nondimensional rate of absorption for two spheres along the flow direction. Pe = 50 *(basis sphere radius).* z_{12} = *variable (in units of sphere radii). The J data refer to* [8]*, the EL data to the current model.*

z	q_J	q_{EL}
2.5	0.69	0.49
4	0.74	0.64
6	0.78	0.74

Juncu [8] studied the temporal evolution of the heat flow rate to two spheres aligned along the flow direction. The flow was assumed to be laminar; the Stimson–Jeffery [15] flow field was used. Most of the calculations were performed at Pe = 100 (basis sphere diameter). Although the emphasis in this paper was on the *unsteady*-state heat equation, some steady-state data were tabulated as well. Just as in many of the aforementioned references, Juncu found that the Nusselt number of both the leading and the trailing spheres were smaller than that of an isolated sphere. Of course, the reduction effect for the trailing sphere was generally larger than for the leading sphere. In Table 6, we have tabulated q_2/q_1, the ratio of the Nusselt number (or absorption rate) between the trailing and the leading spheres.

4.2.1. Discussion of Tables 2 through 6. There are some features of the numerical studies just discussed that are complicating factors in a comparison with our model:

- most of the data were acquired at relatively high Reynolds numbers [16, 17], while our model is a laminar-flow model;
- most of the data refer to relatively low Péclet numbers [3], while our model is a high Péclet number model.

By and large, the agreement between the model and the results of the numerical studies is reasonably satisfactory. None of the deviations is larger than 30%, and most of them are considerably smaller. The deviations are neither systematically positive

TABLE 7
Dependence of the concentration c in the wake zone on the distance z (in units of sphere radius) for Pe = 1000.

z	c
2.5	0.30
4	0.40
5.5	0.50
8.5	0.60
13	0.70
23	0.80
50	0.90
100	0.95

nor negative in sign. Some trends, even though not completely systematic, include the following:

- at small intersphere separations, the EL model tends to underpredict the q-values (normalized absorption rate);
- at relatively low Péclet numbers (say, < 100) and not too small intersphere separations, the model tends to overpredict q;
- at higher Péclet numbers, the model tends to underpredict the q-values.

The underprediction at small intersphere separations is readily explainable. Our model is basically a single-sphere theory that is applied to multiple-sphere clusters. We calculate the interference effect between spheres based on the *unperturbed* wake field of a single sphere. This is the root cause of the problem. If a downstream sphere is very close behind an upstream sphere, clearly the flow field in the interstitial space between the two spheres will not resemble the unperturbed field of an isolated sphere. In the interstitial space between two spheres that almost touch, the flowing medium will be almost stagnant. There, diffusion will be more dominant than in the unperturbed flow field. This is not captured in our model, and this leads to an underprediction of q.

The other two trends mentioned above are not so readily explained.

4.2.2. The case of high Péclet number and large intersphere separation. The numerical studies considered before were characterized by the facts that both the intersphere separations and the Péclet numbers were mostly relatively small (separations < 10 sphere radii; Pe < 100). There is a scarcity of data points with relatively large intersphere separations and large Péclet numbers. This is a pity because it makes it impossible for us to check one of the most interesting (and surprising!) conclusions of the model, namely, that at high Péclet numbers, even at relatively large intersphere separations, the downstream sphere can still have a relatively low absorption rate. As an illustration of this statement, consider the Pe = 1000 curve in Figure 2. Table 7 highlights the data from that figure and clearly demonstrates how slowly the curve approaches its asymptotic value.

One expects the hydrodynamic interactions between two spheres to become gradually less and less important with distance. For center-to-center distances < 10 (sphere radii), the flow field of the upstream sphere would be expected to be relatively unaffected by the presence of a second downstream sphere. It follows that the combination of large intersphere separation and large Péclet number should offer a good opportunity for testing the validity of the current model. For a Péclet-number of 1000, a distance range between, say, 10 and 50 (sphere radii) should be an excellent test range.

5. Conclusions. The convection-diffusion equation has been studied for a single absorbing sphere in a laminar flow field under high Péclet conditions (convection dominant over diffusion). The theory of V. G. Levich has been extended in such a manner that the mathematical and physical inconsistencies in the original model have been corrected. These corrections concern in particular the description of the wake zone of the sphere. The resulting so-called extended Levich model makes it possible to study the interactions between spheres that influence each other's rate of absorption. A sphere that is located on the downstream side of a second sphere is shielded from the flow by the upstream sphere, and its absorption rate might be significantly lower than it would have been without this shielding effect. From a mathematical model of the wake zone of a single sphere, a linear interaction model of multisphere interference effects has been constructed. Model computations show that the spatial range of these interference effects is quite large, generally decaying as distance^{-1} in the wake zone. Depending on the magnitude of the Péclet number, interference effects may be quite significant, even for spheres that are more than 10 sphere radii apart. At Pe = 1000 and at an intersphere separation of 10, the normalized absorption rate of a downstream sphere is as low as ≈ 0.65.

The model was compared against a number of different data sources. For the single-sphere model, numerical simulations were carried out using commercial finite-element software. The discrepancies between the analytical model and the numerical results were mostly $< 10\%$ or considerably lower than 10%. An appreciable part of this discrepancy stems from the original Levich model itself, rather than from our method of extending the Levich model. For multisphere problems, the model was compared against previously published numerical simulation studies [3, 8, 14, 16, 17]. In these comparisons, the discrepancies were found to be $< 30\%$. For relatively small intersphere separations, the model results were generally too low. The most likely cause of the latter observation is the model's failure to account for hydrodynamic interactions between the spheres (flow stagnancy in the space between the spheres). As a result, for this condition, the model overemphasizes the importance of convection and underestimates the effect of diffusion.

One type of test condition for which the numerical studies unfortunately do not contain any data to compare with the model is the combination of large Péclet number (say, $>$ or preferably $\gg 100$) and large intersphere separation (say, > 10, preferably > 20). Under these conditions, the current model predicts surprisingly large effects on the absorption rate. It would be of great value to have independent numerical studies that could be used to validate this aspect of the model.

Appendix A. Justification for neglecting the axial diffusion term in (2.18). Equation (2.18) contains an axial as well as a radial diffusion term. From (2.19) onward, the axial diffusion term was dropped. In this appendix, a justification is given for that simplification.

Referring to the change of variables from $\{\rho, z\}$ to $\{\psi, Z\}$ discussed in section 2.1, the following shorthand notation is used so as to avoid notational clutter:

$$\frac{\partial}{\partial \rho} = \frac{\partial}{\partial \rho}\bigg|_z \; ; \quad \frac{\partial}{\partial z} = \frac{\partial}{\partial z}\bigg|_\rho \; ; \quad \frac{\partial}{\partial \psi} = \frac{\partial}{\partial \psi}\bigg|_Z \; ; \quad \frac{\partial}{\partial Z} = \frac{\partial}{\partial Z}\bigg|_\psi . \tag{A.1}$$

Referring to (2.15), we write

$$\begin{aligned}\frac{\partial^2 c}{\partial z^2} &= \left[\frac{\partial\psi}{\partial z}\frac{\partial}{\partial\psi}+\frac{\partial}{\partial Z}\right]\left[\frac{\partial\psi}{\partial z}\frac{\partial c}{\partial\psi}+\frac{\partial c}{\partial Z}\right] \\ &= \frac{\partial\psi}{\partial z}\frac{\partial}{\partial\psi}\left[\frac{\partial\psi}{\partial z}\frac{\partial c}{\partial\psi}\right]+\frac{\partial\psi}{\partial z}\frac{\partial}{\partial\psi}\left[\frac{\partial c}{\partial Z}\right]+\frac{\partial}{\partial Z}\left[\frac{\partial\psi}{\partial z}\frac{\partial c}{\partial\psi}\right]+\frac{\partial^2 c}{\partial Z^2}.\end{aligned} \tag{A.2}$$

Now, the Z variable is rescaled so that $\epsilon Z = t$, which is the time-like variable in our diffusion equation. Then (A.2) becomes

$$\frac{\partial^2 c}{\partial z^2} = \frac{\partial\psi}{\partial z}\frac{\partial}{\partial\psi}\left[\frac{\partial\psi}{\partial z}\frac{\partial c}{\partial\psi}\right]+\epsilon\,\left\{\frac{\partial\psi}{\partial z}\frac{\partial}{\partial\psi}\left[\frac{\partial c}{\partial t}\right]+\frac{\partial}{\partial t}\left[\frac{\partial\psi}{\partial z}\frac{\partial c}{\partial\psi}\right]\right\}+\epsilon^2\,\frac{\partial^2 c}{\partial t^2}. \tag{A.3}$$

Only the first term on the right-hand side of (A.3) survives when the limit $\epsilon \to 0$ is taken. In this limit, (2.18) therefore becomes

$$\frac{1}{\rho}\frac{\partial\psi}{\partial\rho}\left\{\frac{\partial}{\partial\psi}\left[\rho\frac{\partial\psi}{\partial\rho}\frac{\partial c}{\partial\psi}\right]-\frac{\partial c}{\partial t}\right\}+\frac{\partial\psi}{\partial z}\frac{\partial}{\partial\psi}\left[\frac{\partial\psi}{\partial z}\frac{\partial c}{\partial\psi}\right]=0. \tag{A.4}$$

Since

$$u_z = \frac{1}{\rho}\frac{\partial\psi}{\partial\rho}\ , \quad u_\rho = -\frac{1}{\rho}\frac{\partial\psi}{\partial z} \tag{A.5}$$

(A.4) can be rewritten as

$$u_z\left\{\frac{\partial}{\partial\psi}\left[\rho^2 u_z\frac{\partial c}{\partial\psi}\right]-\frac{\partial c}{\partial t}\right\}+\rho u_\rho\frac{\partial}{\partial\psi}\left[\rho u_\rho\frac{\partial c}{\partial\psi}\right]=0. \tag{A.6}$$

u_z and u_ρ are the axial and the (cylindrical-)radial component of the Stokes velocity field around the central sphere. They are given by

$$u_z = 1-\frac{3}{2r}+\frac{1}{2r^3}+\frac{3}{4}\rho^2\left(\frac{1}{r^3}-\frac{1}{r^5}\right) \tag{A.7}$$

and

$$u_\rho = -\frac{3}{4}\rho\ z\left(\frac{1}{r^3}-\frac{1}{r^5}\right), \tag{A.8}$$

where $r=\sqrt{\rho^2+z^2}$. Contour plots of u_z and u_ρ in the $\{\rho, z\}$-plane (not shown here) show that while u_z tends to unity as $r\to\infty$, $|u_\rho|$ is $<$ or $\ll 0.05$ everywhere except inside two lobes close to the sphere. Even inside those two lobes, its maximum value is quite limited: $\max\left(|u_\rho|\right) = 1/\left(4\sqrt{3}\right) \approx 0.144$.

It is therefore justified to neglect the third term in (A.6) (which depends on u_ρ) as compared to the first term (which depends on u_z). Since $u_z \neq 0$ everywhere in the domain except on the surface of the sphere, the expression within the curly brackets must be $= 0$, which leads to (2.19).

Appendix B. Some words regarding nomenclature used in section 4.2. A few words are in order regarding the nomenclature used in section 4.2. In that section, the results of the current model are compared with the outcomes of various numerical studies [3, 8, 14, 16, 17]. These papers are numerical simulation studies of mass or heat transport to an assembly of absorbing spheres in a flowing medium. The *independent* variables in such studies are the Reynolds number and the Péclet number, while the *dependent* variables are the Sherwood number (in the case of mass transport) or the Nusselt number (in the case of heat transport).

The Reynolds and Péclet numbers are defined in the customary manner:

$$\text{Re} = \frac{a\ u}{\nu} \quad ; \quad \text{Pe} = \frac{a\ u}{D} \quad ; \quad \text{Pe}_T = \frac{a\ u\ \rho_f\ c_p}{\lambda}, \tag{B.1}$$

where u is a characteristic (scalar) velocity of the flowing medium, ν is the kinematic viscosity of the fluid, and D is the diffusion constant of the diffusing species. Pe_T is the thermal analogue of the Péclet number: the mass diffusion constant D is replaced by the thermal diffusivity $\lambda/(\rho_f\ c_p)$, where λ is the thermal conductivity (in SI units: W/(m °C)), while ρ_f and c_p are the mass density and the specific heat of the fluid. The symbol a denotes the size of the absorbing object (in our case, the size of the spheres). Due care must be exercised here: some authors use the sphere's diameter, while others take the sphere's radius. In our model, a is the sphere's radius. References [3, 8, 14, 16, 17], however, use the sphere's diameter, as is more customary in the engineering literature. This leads to differences of a factor 2 between "our" and "their" definitions for Re and Pe.

Section 4.2 also refers to the Prandtl number, defined as

$$\text{Pr} = \frac{\nu\rho_f\ c_p}{\lambda}. \tag{B.2}$$

It is simply related to the Reynolds number and the thermal Péclet number Pe_T:

$$\text{Pe}_T = \text{Pr Re}. \tag{B.3}$$

As regards the *dependent* variables (Sherwood or Nusselt number, as the case may be), the calculated object is the *flux* of mass or heat: the radial derivative of the concentration (or enthalpy) at the surface of the absorbing spheres. This quantity is a function of the angular orientation. In the current study, this aspect is glossed over by integrating the flux over the surface of each one of the absorbing spheres. What remains is a unique number for every sphere in the assembly, usually a different number for each individual sphere. It is desirable to normalize these numbers to a common standard. In our model, this is done by dividing the integrated flux of a particular sphere by the flux this sphere would have in the absence of all the other spheres in the assembly, i.e., when the subject sphere is *not* experiencing the competitive effect of the other members of the cluster. Although the authors of [3, 8, 14, 16, 17] follow a slightly different approach, we can nevertheless compare their results with ours by recalibrating the fluxes of their downstream spheres vis-à-vis the flux of the most upstream member of the cluster.

In the quoted studies [3, 8, 14, 16, 17] sometimes Re was varied, sometimes Pr, and sometimes both. Our model does not depend on Re or Pr, only on their product Pe. The comparisons were always done in such a way that the Péclet numbers in our model and the quoted studies matched.

REFERENCES

[1] M. Abramowitz and I. A. Stegun, *Handbook of Mathematical Functions*, Dover, 1970.

[2] A. Acrivos and T. D. Taylor, *Heat and mass transfer from single spheres in Stokes flow*, Phys. Fluids, 5 (1962), pp. 387–394.

[3] K. Aminzadeh, T. R. Al Taha, A. R. H.Cornish, M. S. Kolansky, and R. Pfeffer, *Mass transport around two spheres at low Reynolds numbers*, Int. J. Heat Mass Transfer, 17 (1974), pp. 1425–1436.

[4] G. K. Batchelor, *An Introduction to Fluid Dynamics*, Cambridge University Press, Cambridge, UK, 1967.

[5] G. K. Batchelor, *Mass transfer from a particle suspended in fluid with a steady linear ambient velocity distribution*, J. Fluid Mech., 95 (1979), pp. 369–400.

[6] J. A. Biello and R. Samson, *Competitive effects between stationary chemical reaction centres: A theory based on off-center monopoles*, J. Chem. Phys., 142 (2015), 094109.

[7] R. Clift, J. R. Grace, and M. E. Weber, *Bubbles, Drops and Particles*, Dover, 1978.

[8] G. Juncu, *Unsteady forced convection heat/mass transfer around two spheres in tandem at low Reynolds numbers*, Internat. J. Thermal Sci., 46 (2007), pp. 1011–1022.

[9] J. H. Knight, J. R. Philip, and R. T. Waechter, *The seepage exclusion problem for spherical cavities*, Water Resources Res., 25 (1989), pp. 29–37.

[10] V. G. Levich, *Physicochemical Hydrodynamics*, Prentice Hall, 1962.

[11] E. E. Michaelides, *Hydrodynamic force and heat/mass transfer from particles, bubbles, and drops: The Freeman Scholar Lecture*, J. Fluids Eng., 125 (2003), pp. 209–238.

[12] J. R. Philip, *The scattering analog for infiltration in porous media*, Rev. Geophys., 27 (1989), pp. 431–448.

[13] J. R. Philip, J. H. Knight, and R. T. Waechter, *Unsaturated seepage and subterranean holes: Conspectus, and exclusion problem for circular cylindrical cavities*, Water Resources Res., 25 (1989), pp. 16–28.

[14] R. S. Ramachandran, C. Kleinstreuer, and T.-Y. Wang, *Forced convection heat transfer of interacting spheres*, Numer. Heat Transfer A, 15 (1989), pp. 471–487.

[15] M. Stimson and G. B. Jeffery, *The motion of two spheres in a viscous fluid*, Proc. Roy. Soc. London Ser. A, 111 (1926), pp. 110–116.

[16] R. Tal, D. N. Lee, and W. A. Sirignano, *Heat and momentum transfer around a pair of spheres in viscous flow*, Int. J. Heat Mass Transfer, 27 (1984), pp. 1953–1962.

[17] J. S. Tsai and A. M. Sterling, *The combustion of a linear droplet array in a convective, coaxial potential flow*, Combust. Flame, 86 (1991), pp. 189–202.

[18] O. C. Zienkiewicz, C. Emson, and P. Bettess, *A novel boundary infinite element*, Internat. J. Numer. Methods Engrg., 19 (1983), pp. 393–404.